JOURNAL OF SPACECRAFT AND ROCKETS
Vol. 43, No. 4, July–August 2006

Aerodynamic Analysis of Grid-Fin Configurations at Supersonic Speeds

P. Theerthamalai* and M. Nagarathinam†
Defence Research and Development Laboratory, Hyderabad 500 058, India

An aerodynamic prediction method for the estimation of aerodynamic characteristics of grid-fin configurations at supersonic Mach numbers has been developed. The method is based on shock-expansion theory. The shock and expansion relations and the interactions between the shock and expansion waves are used to predict the pressure distribution inside each grid-fin cell. The effect of body is modeled using doublet in the crossflow plane. The effect of symmetric separated vortices from the leeward side of body is also modeled using empirical data for the strength and location of vortices. The present method has been validated with available experimental data for body grid-fin configurations at angles of attack without and with fin deflection. The comparison of normal force coefficient on the individual grid fins as well as the overall normal force, pitching moment, and axial force coefficient with experimental data is good. Effect of roll orientation on normal force, pitching moment, and induced out-of-plane force is also brought out.

Nomenclature

C_A	=	axial force coefficient
C_l	=	rolling moment coefficient
C_m	=	pitching moment coefficient
C_N	=	normal force coefficient
$C_{NB(F)}$	=	normal force coefficient on body in presence of fin
$C_{NF(B)}$	=	normal force coefficient on fin in presence of body
C_n	=	yawing moment coefficient
C_S	=	side force coefficient
M	=	Mach number
$\boldsymbol{n}$	=	normal vector to the web, $[n_x\ n_y\ n_z]$
Re	=	Reynolds number based on body diameter
r	=	radial location
r_b	=	body radius
r_c	=	vortex core radius
u_x, u_y, u_z	=	velocity components in x, y, and z directions, respectively
V_∞	=	freestream velocity
α	=	freestream angle of attack
Γ	=	strength of the separated body vortex
δ	=	fin deflection
θ	=	web roll angle with respect to positive y axis
θ_c	=	roll position of web with respect to vortex center
ϕ	=	fin roll angle with respect to positive y axis (ϕ positive toward positive z axis)

I. Introduction

GRID fins are nonconventional aerodynamic control surfaces, which are made of a frame supporting lifting surfaces positioned in the form of a lattice. Russian Federation armed forces earlier used grid fins on the SS-12, SS-20, SS-21, and SS-23 short- and intermediate-range ballistic missiles; AA-12 air-to-air missile; SS-25 mobile intercontinental missile; and 91RE1 underwater-launched antisubmarine ballistic missile. Grid fins are being investigated by other countries for aerodynamic control of highly maneuverable air-launched weapons due to their advantage over conventional planar controls at high angles of attack and high Mach numbers.

The main advantage of the grid fin is low hinge moment due to low chord length, and consequently, the size of the control actuator is small. The other advantages of the grid fin are 1) efficient packaging and suitability for tube launching, 2) good lift characteristics at supersonic speeds, 3) very high stall angle of attack, and 4) high strength-to-weight ratio. The main drawbacks of grid fin are 1) high drag, 2) lower efficiency at transonic speeds, and 3) complex structure.

Prediction methods have been reported for aerodynamic characterization of grid fins. The vortex-lattice method has been used for subsonic flows[1] for linear characteristics and an empirical relation using experimental data for non-linearity.[2] An empirical relation based on experimental data has been used for transonic speeds.[3] Evvard's theory has been used for supersonic flows for linear characteristics and empirical relation using experimental data for non-linearity (see Ref. 4). Most of the prediction methods use body upwash for the effect of the body.

Computational methods have been in use for analyzing the flow features of grid fins,[5,6] the effect of ramp near the grid fin,[7] and comparison of planar and grid fins.[8,9] The effect of the orientation of the individual grid fin with respect to flow direction has also been brought out in the computational studies.

Many wind-tunnel test studies have been reported to study the effect of Mach number, angle of attack, roll angles, grid configuration, grid density, etc.[1,10–14] Free-flight testing in the aeroballastic range has also been conducted for investigation of grid-fin configuration characteristics.[15,16]

This paper presents a prediction method for the aerodynamic characteristics of grid-fin-body configurations without and with fin deflection at arbitrary roll orientations. The prediction methodology and validation with experimental data are presented.

II. Prediction Methodology

The prediction method used for the estimation of aerodynamic characteristics of grid fins without fin deflection is presented in Ref. 17. In this paper, the method is extended for grid fin with fin deflection and at different roll orientations.

The grid fins are divided into their constituent cells. Each cell has three or more webs. The pressure distribution inside the cell can be evaluated, knowing the Mach number, local angle of attack, and flow direction for each cell. Body interference effects and the separated body vortex effect are modeled. The details of the cell force estimation and the body–grid-fin interference are presented in the following sections.

Received 22 March 2005; revision received 16 July 2005; accepted for publication 9 September 2005.

*Scientist, Directorate of Aerodynamics.
†Technology Director, Directorate of Aerodynamics.

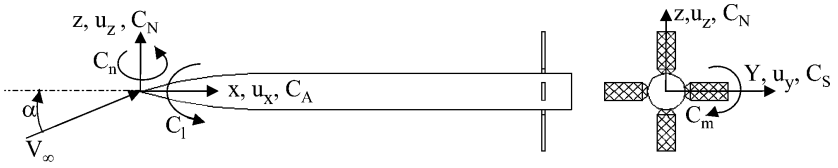

Fig. 1 Axis system and sign convention.

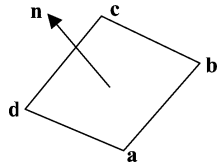

Fig. 2 Web corner points.

A. Grid-Fin Coordinate System and Geometry

The coordinate system is located at the nose of the body with right-hand notation. The x axis is along the body, the y axis is along the right side viewed from the rear, and the z axis is upward as shown in Fig. 1. The grid-fin geometry is divided into cells, and the cells are divided into three or four webs. Fin deflection is modeled by rotation of webs about the hinge line. Roll orientation is modeled by rotation about the x axis. The details of rotation about the hinge line and about the x axis are presented. Consider a single web with corner points at a, b, c, and d. Let x_{ai}, y_{ai}, and z_{ai} be the initial coordinates of point a when the fin is along the y axis (roll angle 0) and without deflection. The coordinates of the point a after deflection by angle δ is given by

$$\begin{aligned} x_{a\delta} &= (x_{ai} - x_{\mathrm{hl}})\cos\delta + z_{ai}\sin\delta + x_{\mathrm{hl}} \\ y_{a\delta} &= y_{ai} \\ z_{a\delta} &= z_{ai}\cos\delta - (x_{ai} - x_{\mathrm{hl}})\sin\delta \end{aligned} \tag{1}$$

where x_{hl} is the axial hinge location of the fin. The coordinates after rotation about the x axis by angle ϕ is given by

$$\begin{aligned} x_a &= x_{a\delta} \\ y_a &= y_{a\delta}\cos\phi - z_{a\delta}\sin\phi \\ z_a &= y_{a\delta}\sin\phi + z_{a\delta}\cos\phi \end{aligned} \tag{2}$$

When the final coordinates of the web corner points are known (Fig. 2) the normal to the web can be evaluated by the following relation:

$$\boldsymbol{n} = \frac{(\boldsymbol{a}-\boldsymbol{c})\times(\boldsymbol{b}-\boldsymbol{d})}{|(\boldsymbol{a}-\boldsymbol{c})\times(\boldsymbol{b}-\boldsymbol{d})|} \tag{3}$$

where $\boldsymbol{a}$, $\boldsymbol{b}$, $\boldsymbol{c}$, and $\boldsymbol{d}$ are the position vectors of corner points of a, b, c, and d.

B. Grid-Fin Cell Characteristics

Pressure distribution inside the cell is obtained using shock-expansion method. Each cell has three or more webs. The pressure on each web of the cell can be obtained using a shock or expansion relation knowing the effective angle of attack normal to the web. At the corner of the cell, there will be interaction of the adjacent webs. The pressure at the interaction region is obtained by shock or expansion of the web surface followed by shock or expansion due to the interfacing web. The region of interaction is calculated using the interfering web surface wave angle. With use of this method, the pressure distribution on the web surfaces and the overall force contribution due to each cell can be estimated. The thickness of the fin web is assumed to be zero for the estimation of pressure distribution and evaluation of forces and moments except axial force.

C. Effect of Body on the Fin Characteristics

The effect of the body on the fin characteristics has been modeled using upwash theory. In upwash theory, the body crossflow field is modeled using a doublet in a freestream flow. The axis system is shown in Fig. 1. The velocity components due to doublet in the crossflow plane are

$$\begin{aligned} u_x &= V_\infty\cos\alpha \\ u_y &= -V_\infty\sin\alpha\sin 2\theta\left(r_b^2/|\boldsymbol{r}|^2\right) \\ u_z &= V_\infty\sin\alpha\left[1+\cos 2\theta\left(r_b^2/|\boldsymbol{r}|^2\right)\right] \end{aligned} \tag{4}$$

where, $\boldsymbol{r}$ is the radial location of the point at which velocity is required. When the velocity components and the unit normal vector to the web are used, the Mach number and the angle of attack faced by the web can be evaluated.

D. Effect of a Body Vortex

According to upwash theory, the leeward side-fin angle of attack and normal force will be almost same as that of windward side. However, the experimental and computational results[9] show that the leeward fin forces are much smaller and negative for high angle of attack compared to the windward fin forces. The reason for the difference is due to the body vortex separation on the leeward side and its influence on the leeward side fin. For proper prediction, the leeward side vortex effect has also to be modeled. The leeward side vortices are modeled using the empirical relation given in Ref. 18, which gives the location and the strength of the vortex as a function of the distance from the point of vortex separation. The point of vortex separation is also given in Ref. 18 as a function of angle of attack. Two symmetric vortices with two image vortices are used for the effect of the body vortices. The vortex core model has been used to maintain realistic induced velocities near the core. The induced velocity in the circumferential direction due to the vortex[19] is given by

$$u_c = (\Gamma/2\pi r)\left\{1-\exp\left[-1.256\left(r^2/r_c^2\right)\right]\right\} \tag{5}$$

where r is the distance between the vortex center and the web center. In addition to vortex core modeling, the maximum induced velocity due to the body vortex is limited to freestream crossflow velocity, $V_\infty\sin\alpha$. The components of velocity due to body vortex are given by

$$u_{\Gamma x} = 0, \qquad u_{\Gamma y} = -u_c\sin\theta_c, \qquad u_{\Gamma y} = u_c\cos\theta_c \tag{6}$$

where θ_c is the roll position of the web center with respect to the vortex center.

E. Effective Angle of Attack

The effective angle of attack on each web is estimated using the velocity components and the unit normal to the web surface. The velocity components at the web midpoint includes the freestream component, body upwash, and body vortex effect and are given by

$$\begin{aligned} u_x &= V_\infty\cos\alpha \\ u_y &= -V_\infty\sin\alpha\sin 2\theta\left(r_b^2/|\boldsymbol{r}|^2\right) - u_c\sin\theta_c \\ u_z &= V_\infty\sin\alpha\left[1+\cos 2\theta\left(r_b^2/|\boldsymbol{r}|^2\right)\right] + u_c\cos\theta_c \end{aligned} \tag{7}$$

The normal velocity to the web surface is given by the vector dot product of $\boldsymbol{u}$ and $\boldsymbol{n}$, $\boldsymbol{u}\circ\boldsymbol{n} = [u_x\ \ u_y\ \ u_z]\circ[n_x\ \ n_y\ \ n_z]$. The effective angle of attack is given by

$$\alpha_e = \sin^{-1}[(\boldsymbol{u}\circ\boldsymbol{n})/V_\infty] \tag{8}$$

F. Carryover Force on the Body Due to Fin

The carryover force on the body has been modeled using method of images of all of the lifting elements of the fin. Consider a lifting element ABCD outside the body with radius r_b. The radial locations

of the corner points are r_A, r_B, r_C, and r_D. The radial locations of the image points are given by

$$r'_A = r_b^2/r_A, \qquad r'_B = r_b^2/r_B, \qquad r'_C = r_b^2/r_C, \qquad r'_D = r_b^2/r_D \tag{9}$$

Then the carryover force normal to the image lifting element (Fig. 3) is given by

$$C_{N_{B(F)}} = C_{N_{F(B)}} \frac{\text{area of image element}}{\text{area of real lifting element}} \tag{10}$$

G. Fin Axial Force Coefficient

Fin axial force is estimated at zero angle of attack and is assumed to be same at angles of attack. The general shape of the grid-fin cross section is of constant thickness flat plate. Therefore, the axial force is composed of skin-friction drag, leading-edge drag, and trailing-edge base drag. The method given in Ref. 19 is used for the estimation of the drag components.

H. Body Aerodynamic Characteristics

The body aerodynamic characteristics are predicted using Ref. 20, and the method is briefly presented here. The body normal force and pitching moment are estimated using second-order shock-expansion theory for the linear component and crossflow theory for the nonlinear component. The axial force is estimated as the addition of skin-friction drag and wave drag. The body skin-friction drag is evaluated taking the body-wetted area and flat plate skin-friction coefficient. The wave drag of the body is based on second-order shock-expansion theory.

Based on the these modeling aspects, a prediction code for the aerodynamic analysis of configuration with grid fins has been developed.

III. Validation with Experimental Data

The developed prediction code has been applied to three different configurations, and the results obtained are compared with available experimental data. All of the aerodynamic coefficients are normalized with the body cross-sectional area as the reference area, the body diameter as the reference length, and the moment reference point is the nose tip.

A. Configuration 1

Configuration 1 (Fig. 4) is taken from Ref. 9 for which experimental results are available. The repeatability of the experimental data is reported to be within 1% over the test angle-of-attack range. The predicted normal force and pitching moment coefficients are shown in Fig. 5 along with experimental results for Mach number of 2.5 and Reynolds number of 1.2×10^6 based on body diameter. The predicted values are in good agreement with the experimental data, and the deviation is within 10% of the experimental values. The individual grid-fin characteristics are shown in Fig. 6 along with the experimental data. The comparison shows that the predicted values are in good agreement with experiment. It can also be seen that the leeward fin normal force is negative at higher angles of attack, and this trend has also been predicted very well. The predicted axial force coefficient is compared with the experimental values in Fig. 7. The comparison is good, and the maximum deviation is less than 10%.

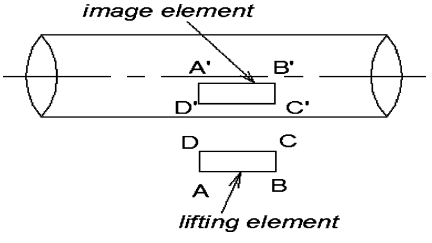

Fig. 3 Carryover force on body due to fin.

B. Configuration 2

Configuration 2 (Fig. 8) is taken from Ref. 10 for which experimental results are available. The quoted accuracy of the fin balance used for the experiment is 2.5% of the rated loads. However, the

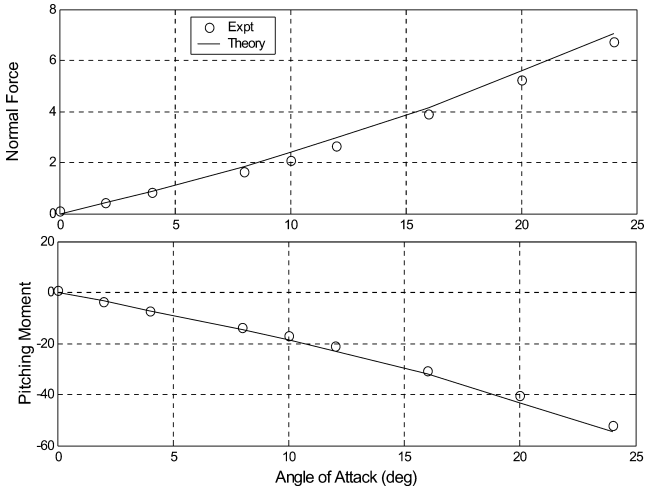

Fig. 5 Predicted overall normal force and pitching moment coefficient compared with experiment (Ref. 9), Mach number 2.5 and Reynolds number 1.2×10^6, configuration 1.

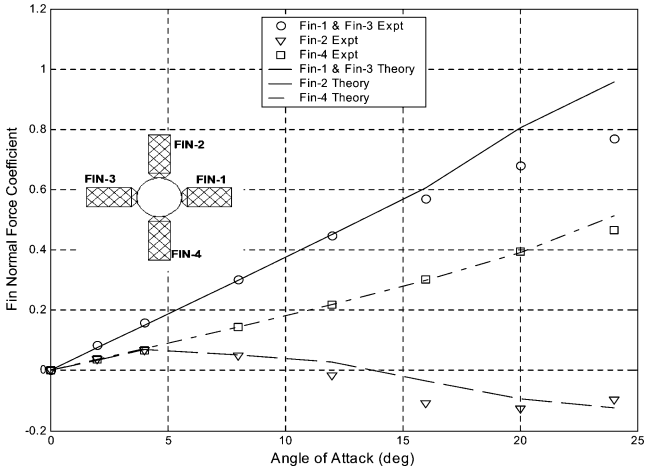

Fig. 6 Predicted individual fin normal force coefficient compared with experiment for configuration 1.

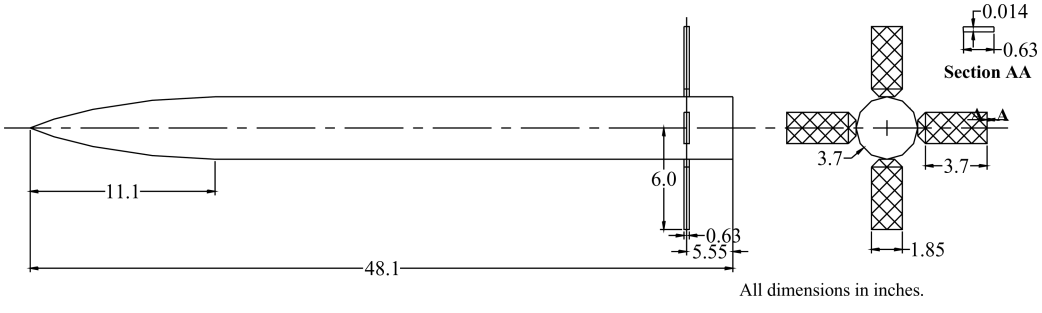

Fig. 4 Configuration 1.

repeatability is within 1% of the rated loads. The predicted normal force coefficient of the horizontal fin is shown in Fig. 9 along with experimental results for Mach numbers of 1.8, 2.5, and 3.5 and test Reynolds numbers of 2.3×10^6, 3.0×10^6 and 4.7×10^6, respectively. The predicted values are in good agreement with the experimental data for Mach numbers of 2.5 and 3.5. However, for Mach number 1.8, the theory overpredicts by around 30% for angles of attack above 7.5 deg. The higher deviation may be due to strong interaction between the shock wave and expansion at low supersonic Mach numbers and shock reflection from the opposite webs.

Fin normal force coefficient with deflection of −15 deg is compared with experimental data in Fig. 10 for Mach numbers 1.8 and 3.5. The comparison for Mach number 1.8 is good for positive angles attack, and the deviation of prediction from experimental data is high for negative angle of attack. The reason for higher deviation for negative angle of attack is probably due to higher effective angle of attack, which causes shock detachment and reflection from the opposite sides. The comparison of prediction with experiment at Mach number 3.5 is good for both positive and negative angles of attack. The better comparison at Mach number of 3.5 is due to attached shock and lower shock angle. At Mach number 3.5, the normal force increment due to surface deflection increases with decrease in angle of attack due to higher effective angle of attack. As the effective angle of attack increases, the pressure after the oblique shock increases nonlinearly, causing a higher increment in the negative angle of attack.

The comparison of predicted axial force coefficient with experiment[21] is shown in Fig. 11. The reported repeatability accuracy of axial force measurement is 0.1 lb (0.45 N), which is around 1.0% of the measured axial force. The axial force coefficient reduces with Mach number, as expected. The predicted axial force coefficient is less than the experimental data, and the difference is less than 10%.

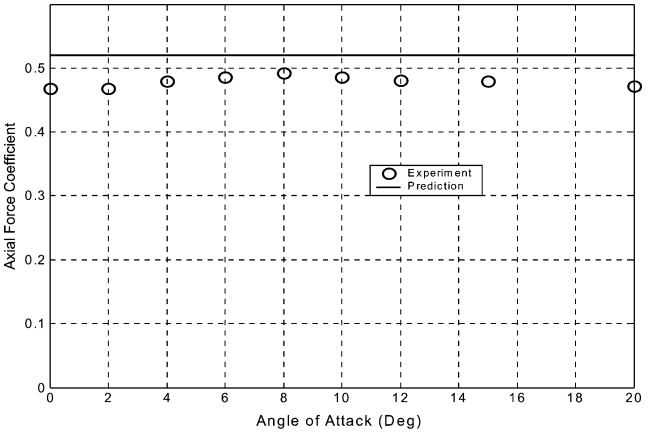

Fig. 7 Predicted overall axial force coefficient compared with experiment (Ref. 9), Mach number 2.5 and Reynolds number 1.2×10^6, configuration 1.

C. Configuration 3

Configuration 3 (Fig. 12), for which experimental results are available, is also taken from Ref. 10. The predicted normal force coefficient of the horizontal fin is shown in Fig. 13, along with experimental results for Mach numbers of 1.8, 2.5, and 3.5. The predicted values are in good agreement with the experimental data for Mach numbers 2.5 and 3.5. However, for Mach number 1.8, the theory overpredicts by around 15% for angles of attack above 7.5 deg.

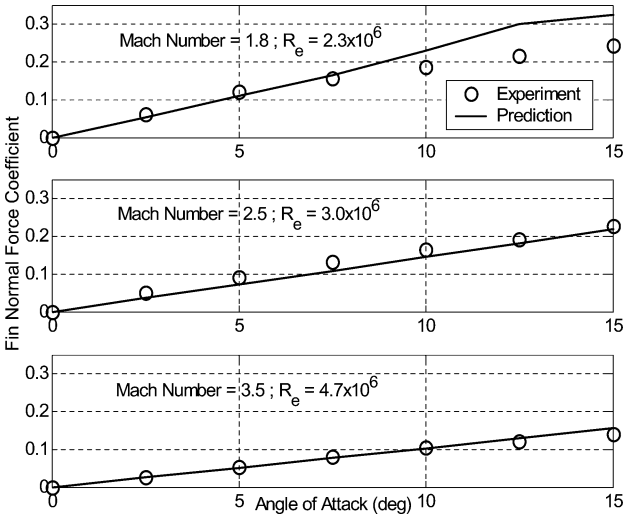

Fig. 9 Predicted horizontal fin normal force coefficient compared with experiment (Ref. 10), configuration 2.

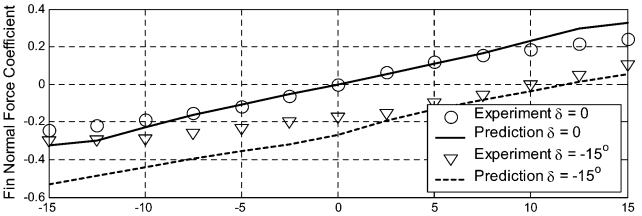

a) Mach number 1.8

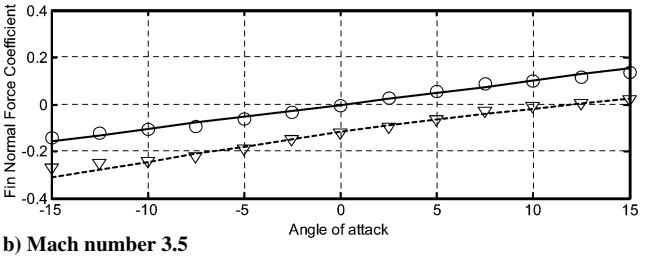

b) Mach number 3.5

Fig. 10 Horizontal fin normal force coefficient with deflection, configuration 2.

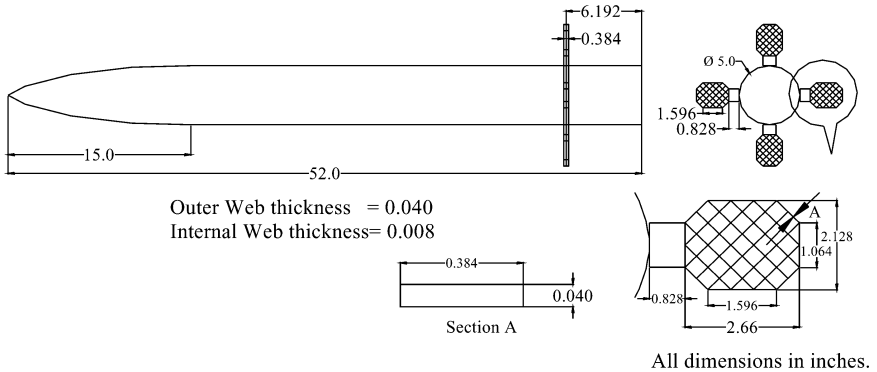

Fig. 8 Configuration 2.

The fin normal force coefficient with deflection of −15 deg is compared with experimental data in Fig. 14 for Mach numbers 1.8 and 3.5. The comparison for Mach number 1.8 is good for positive angles attack, and the deviation of the prediction from experimental data is high for negative angle of attack. The reason for higher deviation in negative angle of attack is due to higher effective angle of attack and shock detachment and reflection from the opposite sides. The comparison is good for Mach number 3.5 for positive and negative angles of attack. The increment in fin normal force coefficient due to surface deflection is higher at higher negative angles of attack due to higher effective angle of attack and associated nonlinearity as explained for configuration 2.

The reason for better comparison for configuration 3 as compared to configuration 2 is probably due to less grid density and low interference of the adjacent web in configuration 3.

D. Effect of Roll Orientation

Most of the experimental data on grid fin configuration available in the literature are generated for cruciform (+) configuration only, and hence, the roll orientation effect could not be validated. The effect of roll orientation has been studied for configuration 1. The overall normal force and pitching moment with angle of attack are shown in Fig. 15 for roll orientation of 0, 22.5, and 45 deg. The roll orientation of 45 deg (× configuration) yields around 10% higher normal force and pitching moment compared to roll orientation 0 (+ configuration). The lateral aerodynamic coefficients at roll angles of 0 and 45 deg are zero due to pitch plane symmetry. The induced lateral characteristics, C_S, C_n, and C_l, for a roll angle of 22.5 deg are shown in Fig. 16. The values of C_S, C_n, and C_l are zero up to an angle of attack of 4 deg, because the body vortex separation starts around 5 deg. The side force and yawing moment coefficients are within 5% of the corresponding normal force and pitching moment coefficients. The values of C_S, C_n, and C_l increase up to an angle of attack of 16 deg and reduces on further increase in angle of attack. This trend is due to relative position of separated body vortex with respect to the fin location.

The fin normal force with roll position is shown in Fig. 17 for different angles of attack. The fin normal force coefficient is high and nearly constant for roll angles from −20 to +40 deg. The normal force on the windward side fin is about 50% of the side fins. The normal force on the leeward side fin is very small compared to the windward side and even negative for higher angles of attack. The induced side force coefficient of the fin with roll position is shown in Fig. 18. The fin side force is nonzero for zero roll angle due to asymmetry of the flow about yaw plane and separated body vortex effect. The maximum side force is observed near a roll orientation of −45 deg (windward side). The side force increases with increase in angle of attack on the windward side. However, the variation is not systematic in the leeward side due to the effect of separated body vortices.

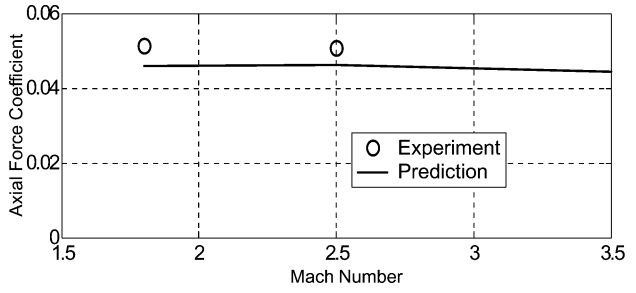

Fig. 11 Predicted axial force coefficient compared with experiment (Ref. 21) for configuration 2.

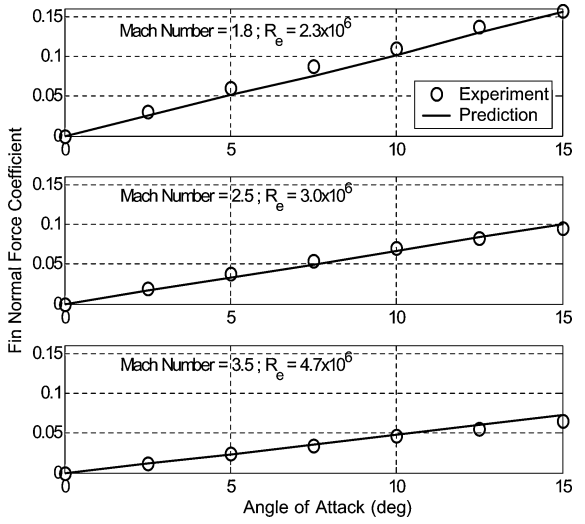

Fig. 13 Predicted horizontal fin normal force coefficient compared with experiment, configuration 3.

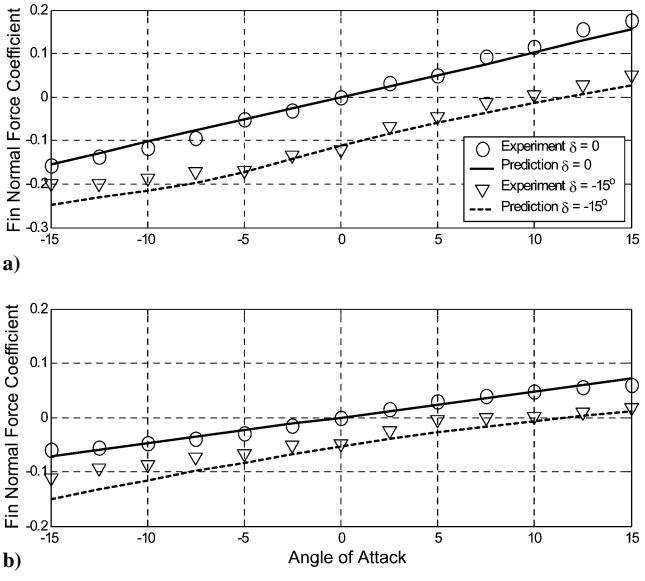

Fig. 14 Horizontal fin normal force coefficient with deflection, configuration 3.

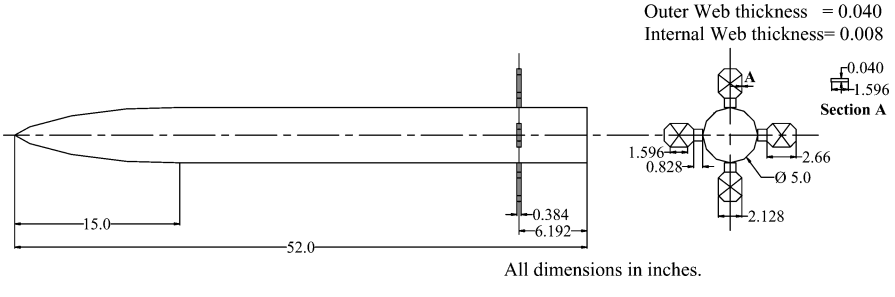

Fig. 12 Configuration 3.

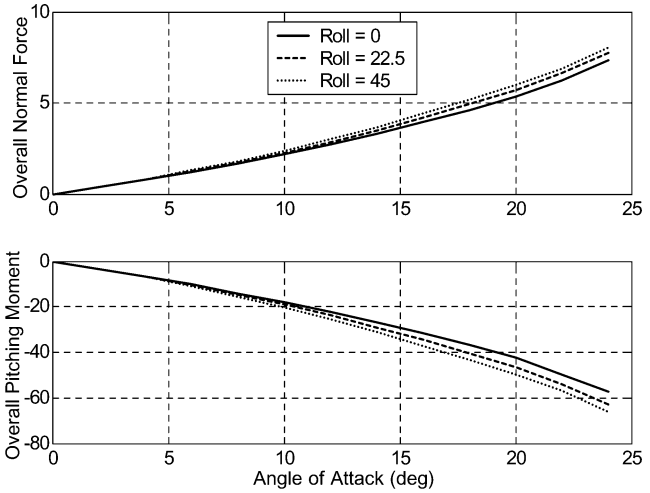

Fig. 15 Overall normal force and pitching moment coefficient for different roll orientations, configuration 1.

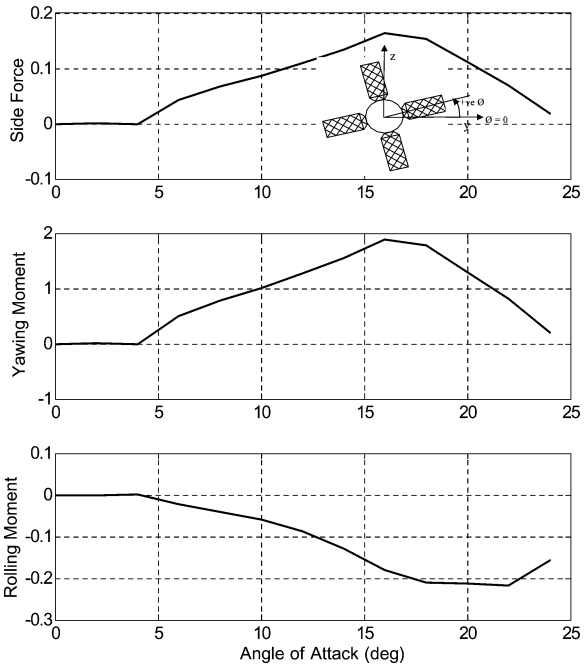

Fig. 16 Side force, yawing moment, and rolling moment coefficient at Mach number 2.5 and roll orientation 22.5 deg, configuration 1.

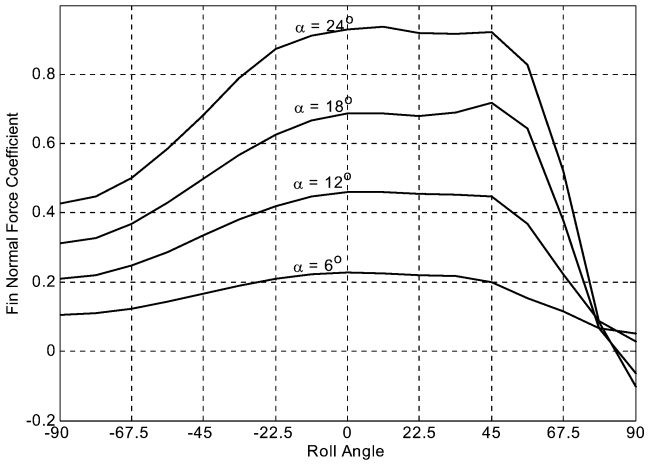

Fig. 17 Fin normal force coefficient with roll angle, configuration 1.

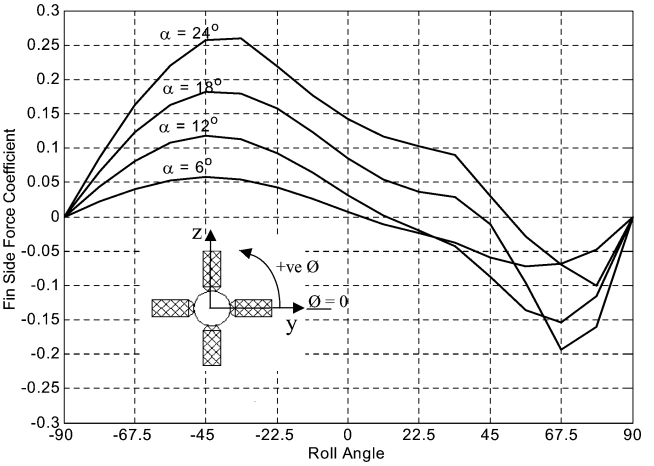

Fig. 18 Fin side force coefficient with roll angle, configuration 1.

IV. Conclusions

A prediction code for the estimation of aerodynamic characteristics of grid-fin configurations without and with fin deflection at angles of attack has been developed. This code can predict the grid-fin characteristics at arbitrary roll orientations. The method is based on shock-expansion theory. The effect of body and body vortices are modeled. The predicted characteristics are compared with available experimental results and the comparison demonstrated the following conclusions:

1) Overall normal force and pitching moment comparison is good.

2) Individual grid-fin characteristics are also predicted well in all of the cases, except for the case of high grid density in low supersonic speeds.

3) The leeward fin characteristics are also predicted well because of the modeling of the separated body vortices.

4) Prediction of fin deflection characteristics is also good for higher Mach numbers. For lower supersonic Mach numbers, the deviation is greater due to high effective angle of attack leading to shock detachment and shock reflection from opposite side webs.

5) More detailed interaction between the shock waves and expansion fans are to be taken into account to improve the accuracy of prediction, especially at lower supersonic Mach numbers and higher effective angles of attack.

6) The effect of roll orientation could not be validated due to lack of experimental data. However, the roll orientation effect is brought out in this study. The induced lateral characteristics are also predicted and presented.

References

[1]Brooks, R. A., and Burkhalter, J. E., "Experimental and Analytical Analysis of Grid Fin Configurations," *Journal of Aircraft*, Vol. 26, No. 9, 1989, pp. 885–887.

[2]Burkhalter, J. E., Hartfield, R. J., and Leleux, T. M., "Nonlinear Aerodynamic Analysis of Grid Fin Configurations," *Journal of Aircraft*, Vol. 32, No. 3, 1995, pp. 547–554.

[3]Kretzschmar, R. W., and Burkhalter, J. E., "Aerodynamic Prediction Methodology for Grid Fins," Proceedings of the NATO RTO Applied Vehicle Technology Panel Symposium on Missile Aerodynamics, RTO-MP-5, NATO Research and Technology Organization, Nov. 1998, pp. 11.1–11.11.

[4]Burkhalter, J. E., "Grid Fins for Missile Application in Supersonic Flow," AIAA Paper 96-0194, Jan. 1996.

[5]Khalid, M., Sun, Y., and Xu, H., "Computation of Flows past Grid Fin Missiles," Proceedings of the NATO RTO Applied Vehicle Technology Panel Symposium on Missile Aerodynamics, RTO-MP-5, NATO Research and Technology Organization, Nov. 1998, pp. 12.1–12.11.

[6]Lin, H., Huang, J. C., and Chieng, C.-C., "Navier–Stokes Computations for Body/Cruciform Grid Fin Configuration," *Journal of Spacecraft and Rockets*, Vol. 40, No. 1, 2003, pp. 30–38.

[7]Chen, S., Khalid, M., Xu, H., and Lesage, F., "A Comprehensive CFD Investigation of Grid Fins as Efficient Control Surface Devices," AIAA Paper 2000-0987, Jan. 2000.

[8]Sun, Y., and Khalid, M., "A CFD Investigation of Grid Fin Missiles," AIAA Paper 98-3571, July 1998.

[9]DeSpirito, J., Edge, H. L., Weinacht, P., Sahu, J., and Dinavahi, S. P. G., "CFD Analysis of Grid Fins for Maneuvering Missiles," AIAA Paper 2000-0391, Jan. 2000.

[10]Washington, W. D., and Miller, M. S., "Grid Fins—A New Concept for Missile Stability and Control," AIAA Paper 93-0035, Jan. 1993.

[11]Washington, W. D., Booth, P. F., and Miller, M. S., "Curvature and Leading Edge Sweep Back Effects on Grid Fin Aerodynamics," AIAA Paper 93-3480, Aug. 1993.

[12]Simpson, G. M., and Sadler, A. J., "Lattice Controls: A Comparison with Conventional, Planar Fins," Proceedings of the NATO RTO Applied Vehicle Technology Panel Symposium on Missile Aerodynamics, RTO-MP-5, NATO Research and Technology Organization, Nov. 1998, pp. 9.1–9.10.

[13]Fournier, E. Y., "Wind Tunnel Investigation of a High L/D Projectile with Grid-Fin and Conventional Planar Control Surfaces," *Proceedings of 19th International Symposium of Ballistics*, Vol. 1, Casino Kursaal Congress Center, Interlaken, Switzerland, 2001, pp. 511–520.

[14]Dupuis, A., and Berner, C., "Aerodynamic Aspects of a Grid Finned Projectile at Subsonic and Supersonic Velocities," *Proceedings of 19th International Symposium of Ballistics*, Vol. 1, Casino Kursaal Congress Center, Interlaken, Switzerland, 2001, pp. 495–502.

[15]Gregg, A., Gerald, W., and Wayne, H., "Transonic Aerodynamic and Scaling Issues for Lattice Fin Projectiles Tested in a Ballistics Range," *Proceedings of 19th International Symposium of Ballistics*, Vol. 1, Casino Kursaal Congress Center, Interlaken, Switzerland, 2001, pp. 413–420.

[16]Gregg, A., Ralf, D., and Wayne, H., "Subsonic/Transonic Free Flight Tests of a Generic Missile with Grid Fins," AIAA Paper 2000-0937, Jan. 2000.

[17]Theerthamalai, P., Manisekaran, S., and Nagarathinam, M., "A Prediction Method for Aerodynamic Characterization of Grid-Fin Configurations at Supersonic Speeds," AIAA Paper 2005-4967, June 2005.

[18]Mendenhall, M. R., and Nielsen, J. N., "Effect of Symmetrical Vortex Shedding on the Longitudinal Aerodynamic Characteristics of Wing–Body–Tail Combinations," NASA CR-2473, Jan. 1975.

[19]Mendenhall, M. R., Perkins, S. C., Jr., and Lesieutre, D. J., *Tactical Missile Aerodynamics: Prediction Methodology*, Vol. 142, Progress in Astronautics and Aeronautics, edited by M. R. Mendenhall, AIAA, Washington, DC, 1992, Chap. 1.

[20]Panneerselvam, S., Theerthamalai, P., Balu, G., Sharma, R. K., Sarkar, A. K., and Balachandran, N., "Aerodynamic Prediction Code for Rapid Design and Analysis of Missile Configurations," *Journal of the Aeronautical Society of India*, Vol. 40, No. 4, 1988, pp. 229–240.

[21]Miller, M. S., and Washington, W. D., "An Experimental Investigation of Grid Fin Drag Reduction Techniques," AIAA Paper 94-1914, June 1994.

M. Miller
Associate Editor